Supplementary Information

Towards characterization of DNA structure under physiological conditions *in vivo* at the single-molecule level using single-pair FRET

Tomáš Fessl[#,‡], František Adamec[#,‡], Tomáš Polívka[#,‡], Silvie Foldynová-Trantírková[‡], František Vácha[#,‡,]* and Lukáš Trantírek[§]*

[#]University of South Bohemia, Faculty of Sciences, Branišovská 31, 37005 České Budějovice, Czech Republic

[‡]Biology Centre ASCR, v.v.i., Branišovská 31, 370 05 České Budějovice

[§]Department of Chemistry, Utrecht University, Padualaan 8, 3584 CH Utrecht, The Netherlands

* **Corresponding author**: vacha@jcu.cz, l.trantirek@uu.nl

Keywords: in-cell FRET; fluorescence; DNA; nucleic acid; ATTO; in vivo

Theory

The FRET efficiencies in Figure S4 were calculated as follows:

$$E_{FRET} = \left[1 + \left(\frac{R}{R_0}\right)^6\right]^{-1}, \qquad \text{(Eq. S1)}$$

Where R_0 represents Főrster radius and R represents inter-probe separation calculated as a size of vector joining donor and acceptor transition dipole moments of dyes attached to DNA. FRET efficiency was measured via fluorescence lifetimes:

$$E_{FRET} = 1 - \tau'_D / \tau_D, \qquad \text{(Eq. S2)}$$

where τ'_D and τ_D are the donor fluorescence lifetimes with and without acceptor. The fluorescence lifetime of individual dyes is an intrinsic property of the molecule, affected only by its chemical environment. In contrast, the detected fluorescence intensity, which is used as more common FRET measurement technique in microscopy, is an extrinsic quantity, which depends on many experimental factors, such as excitation intensity, collection efficiency, and position of the dye with respect to the excitation beam, all of which do not report on the actual dye properties (45).

Interprobe distance PDF derived from simulated dye positions was calculated as:

$$\langle R_{DA} \rangle = \langle |R_D - R_A| \rangle, \qquad \text{(Eq. S3)}$$

where $<R_{DA}>$ is integral interprobe distance accounting for all possible positions of the two dyes (R_D and R_D).

The precision of FRET measurement in the terms of κ^2, was defined as the variance of possible values of orientation factor (Figure S1).

$$\mathrm{Pr}ecision = \left[\mathrm{var}\left(\left(3/2\kappa^2\right)^{1/6}\right)\right]^{1/2} \qquad \text{(Eq. S4)}$$

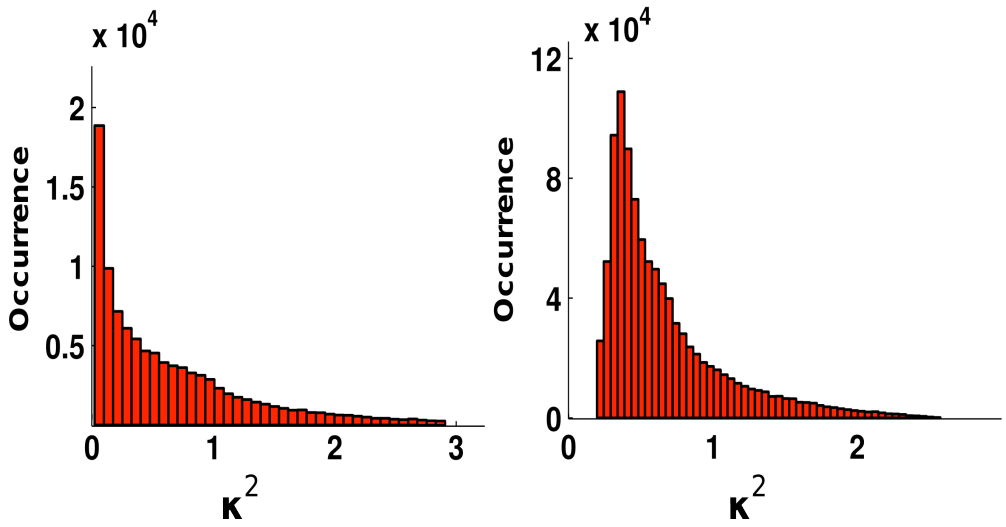

Figure S1. Orientation factor distribution simulated from parameters measured in lysate (*left panel*) and in buffer A (*right panel*).

R_0 PDF (Figure S4) can be derived from distribution of orientation factor using Eq. S4

$$R_0 = 8{,}8 \cdot 10^{-28} \left(\kappa^2 n^{-4} Q_0 J\right), \qquad \text{(Eq. S5)}$$

where *n* is refractive index Q_0 is quantum yield of ATTO680 and *J* is spectral overlap between absorption spectrum of ATTO740 and fluorescence spectrum of ATTO680. Parameters used to calculate particular R_0 in lysate and *buffer A* are listed in Table S3. κ^2 was simulated from donor and acceptor anisotropies (Figure S3) according to Dale et al. (21). *J* was calculated as:

$$J = \int f_D(\lambda)\varepsilon_A(\lambda)\lambda^4 d\lambda\,, \qquad \text{(Eq. S6)}$$

where f_D is normalized fluorescence spectrum of ATT0680 and ε_A is extinction coefficient of ATTO740.

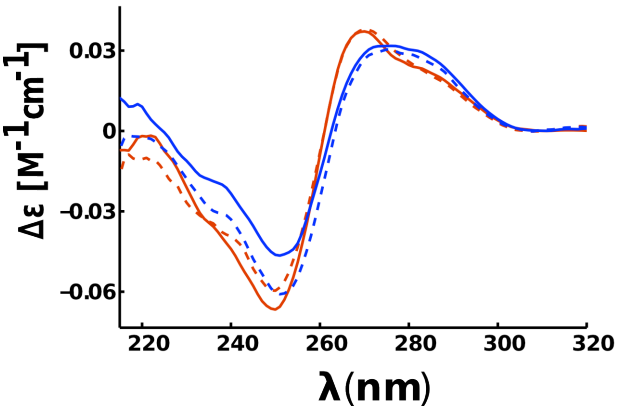

Figure S2. The CD spectra of d(CCTGCACGACCTGTGG).d(CCACAGGTCGTGCAGG) unmodified (red dashed line), modified with ATTO740 (red solid line), with ATTO680 (blue solid line), and with both ATTO680 and ATTO740 (blue dashed line). The spectra were acquired at room temperature in *buffer A*. The spectra were normalized to the DNA concentration.

Optimized protocol for incorporation of fluorescently labeled DNA into E. coli cells

1.) 3µl 0.5 µM DNA into 50µl BL21 E. coli suspension
2.) incubate for 40 min. on ice
3.) incubate for 30 s at 42°C
4.) add 250 µl of pre-warmed SOC (20 g/l bacto-tryptone, 5 g/l bacto-yeast extract, 8.6 mM NaCl, 1M KCl, 1M glucose, pH=7)
5.) shake at 37°C, 225 RPM for 45 min
6.) add 500 µl of PBS, centrifuge at 3000 RPM for 10 min
7.) repeat step 6

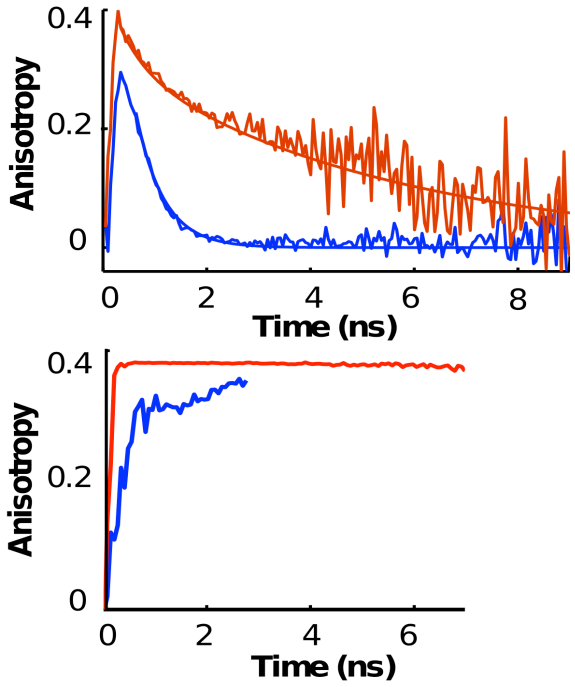

Figure S3. Time-resolved fluorescence anisotropy decays of DNA constructs labelled with ATTO680 (*red line*) and ATTO740 (*blue line*) in *buffer A* (*upper panel*) and in crude bacterial lysate (*bottom panel*). Decays obtained in *buffer A* were deconvoluted and fitted to a multi-exponential model. For the DNA tagged with ATTO 680, the anisotropy of the ATTO680 decayed to zero rapidly with two time components, fast (τ_1= 1.9 ns), which prevails for almost 90% of the total amplitude, and slow (τ_2= 14.9 ns). While fast kinetics can be ascribed to the segmental motion of almost freely rotating dye, the slow component corresponds to the global motion of the dye firmly joined to the DNA duplex. In contrast to the situation for ATTO680, the measured anisotropy decay for the ATTO740 tagged construct contains significant contribution from the slow component, suggestive of a hindered fluorophore rotation. In agreement with this interpretation, the anisotropy did not decay to zero during the time window of the experiment. The ratio between the segmental to global motion was close to 1 (1.11). While the long time components of the double-exponential decays for ATTO680 and ATTO740 were virtually identical, the short time component of ATTO 680 (1.9 ns) was slightly longer than that of ATT0 740 (1.5 ns). Anisotropies in bacterial lysate show complex behavior. Expectedly the anisotropy decay of ATTO680 is much slower due to higher viscosity of lysate. In addition, the construct labeled with ATTO740 shows associated anisotropy decay behavior most likely due to enhanced formation of transient hydrophobic complexes in heterogeneous crude lysate environment compared to diluted buffer A (46). This explanation is in agreement with CD and melting temperature data both indicating transient association of ATTO740 with DNA under diluted conditions. In crude bacterial lysate this association appears to be enhanced.

Table S1. Experimentally determined values of melting temperatures from temperature-induced changes monitored via Δε at 250 and 251 nm.

	DNA[a]	DNA[a]-ATTO680	DNA[a]-ATTO740	DNA[a]-ATTO680/ATTO740
T_m [ºC]	54.8	52.3	56.7	54.9

[a] d(CCTGCACGACCTGTGG).d(CCACAGGTCGTGCAGG)

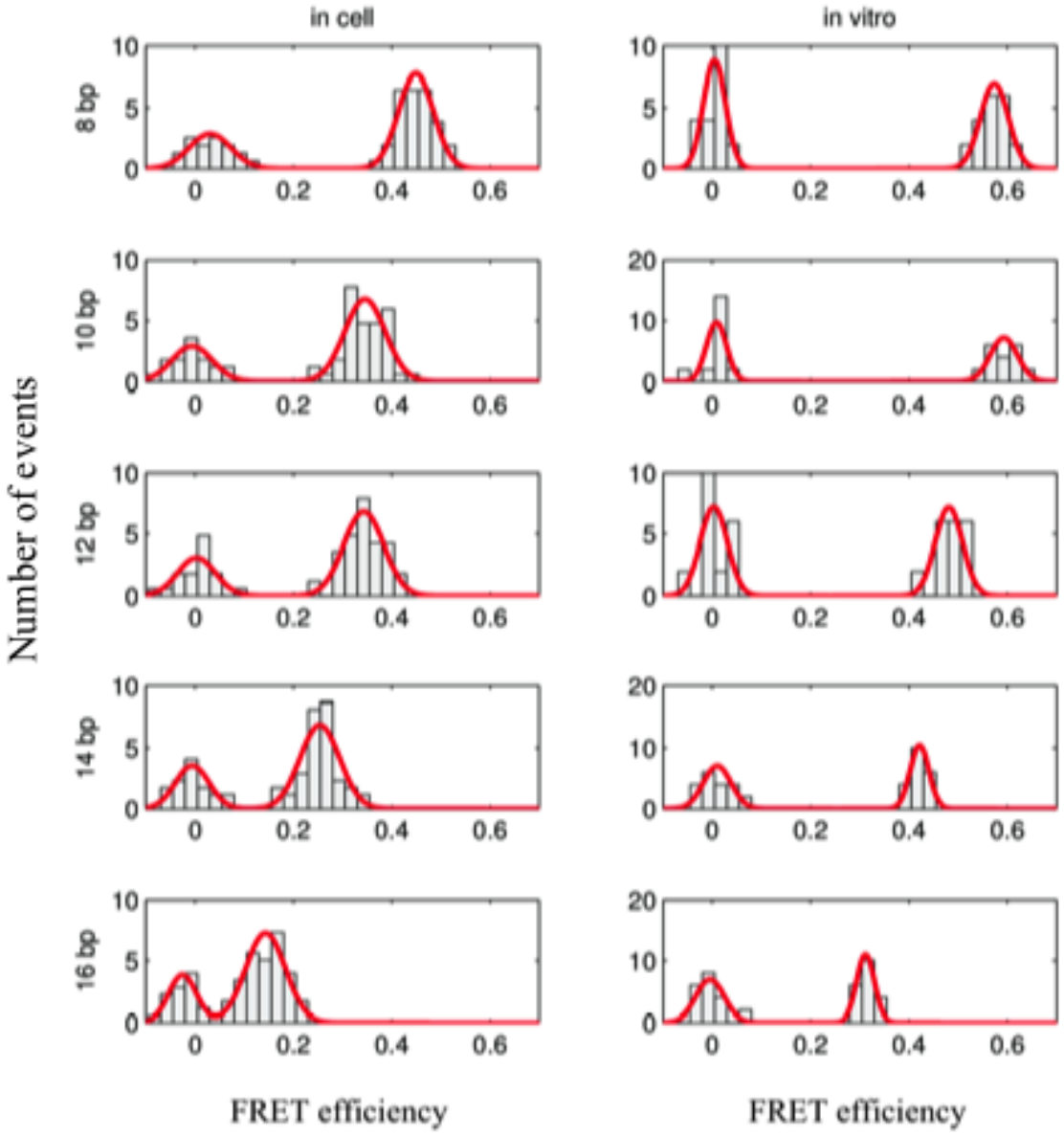

Figure S4: FRET efficiency occurrences (number of events) *in vitro* (left) and *in vivo* (right) as a function of the helix length (gray bars) and their mixed gaussian fits (red curves). Data sets were fitted using maximum likelihood estimation method to explore probability distributions. FRET efficiencies *in vivo* were acquired from single-molecule measurements, in contrast to *in vitro* data, which were collected within repeated ensemble experiments. Ensemble fluorescence decays were treated using the same procedure, which is described for single-molecule data, usually resulting in two lifetime kinetics per one ensemble measurement.

Table S2: Means and standard deviations of FRET efficiency probability distributions shown in Figure S4. FRET was calculated from fluorescence lifetimes, which are determined with two significant digits accuracy. Every mean value is calculated from less than 50 measurements (some values lie in the zero efficiency peak), thus we report FRET efficiencies with maximally three significant digits. This number is based on rule of rounding of division (applied in Eq. S2) and rule for mean value of small data sets (47).

DNA [bp]	**Mean E_{FRET}**	
	in cell	**in vitro**
8	0.449	0.573
10	0.345	0.593
12	0.343	0.481
14	0.253	0.421
16	0.143	0.311

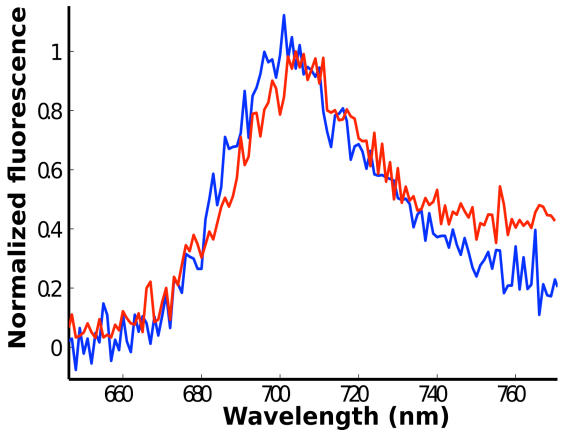

Figure S5. Comparison of ATTO680 fluorescence spectra measured in crude bacterial lysate (*red line*) and inside intact bacterial cell (*blue line*).

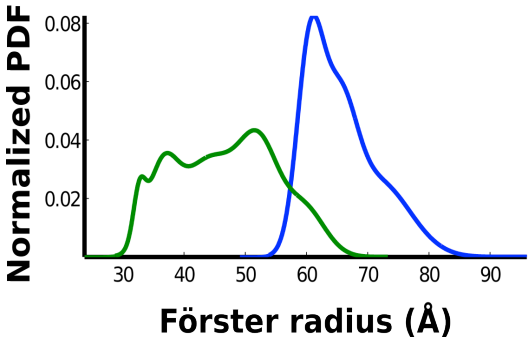

Figure S6. R_0 distribution derived using spectroscopic parameters measured in the crude bacterial lysate (*green line*) and in buffer A (*blue line*). The parameters are listed in Table S3.

Table S3. Acquired spectroscopic parameters used to calculate Förster radius in crude bacterial lysate and in *buffer A* (cf. Materials and Methods)

Environment	**Bacterial lysate**	**Buffer A**
Q_0 **- Quantum yield of ATTO680**	0.1	0.3
ε_A **- Molar absorption coefficient of ATTO740 (L mol^{-1}cm^{-1})**	99000	120000
n - Environment refractive index	1.40	1.33
r_A - Fluorescence anisotropy of ATTO740	0.33	0.22
r_D - Fluorescence anisotropy of ATTO680	0.39	0.18
R_{iso} - Isotropic Förster radius [where $\kappa^2 = 2/3$] (Å)	50.3	67.0

Technical notes: Mean photostability of ATTO680 inside *E. coli* cell was 37 s. Photostability of ATTO740 was usually longer. The photostabilities were determined using the time lapses of CCD images for several individual molecules. *In vivo*, mean number of detected photoelectrons for ATTO680 molecule per 30 s on single photon counting avalanche photodiode (Perkin Elmer, SPCM-AQR-16) was 8 214 counts after background subtraction. Signal produced by individual ATTO740 molecules detected in donor channel after 30 s of data acquisition was hidden under the sum of usual background and noise (measured in the absence of fluorescent probes). For the purpose of the evaluation, the signal from ATTO740 was neglected.

Table S4. Comparison of fluorescence lifetimes measured in crude bacterial lysate and in living bacterial cell. Lifetimes in lysate were determined from 10 independent bulk measurements. Lifetimes in bacterial cells were measured on single molecule level. Mean value is determined from approximately 100 molecules (independent measurements).

	Lifetime mean ± S.D. (ns)	
Environment	***Bacterial lysate***	***E. coli***
ATT0680	1.61 ± 0.12	1.62 ± 0.24
ATT0740	0.5 ± 0.05	0.51 ± 0.21

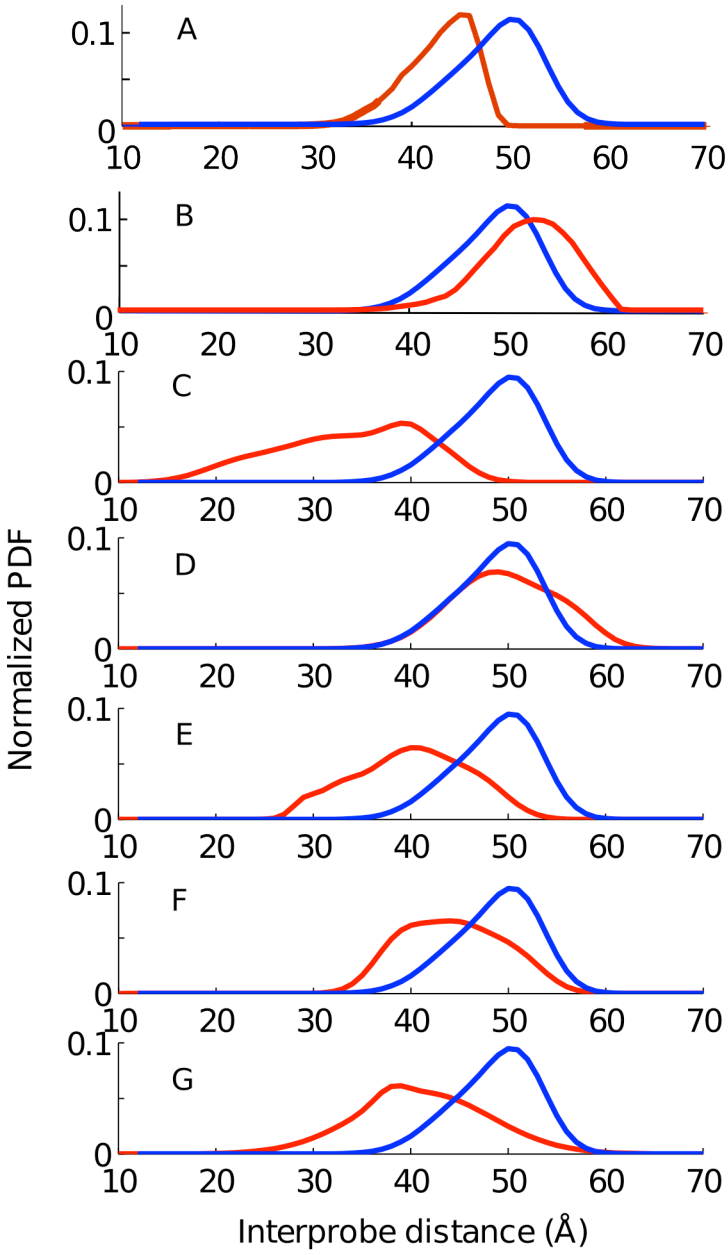

Figure S7. Comparison of simulated inter-probe PDFs between B-DNA (*blue line*), expected DNA conformation inside a cell, and alternative DNA structures (*red line*) representing canonical A-DNA (A), canonical Z-DNA (B), DNA bound to protein (PDB ID:1QUM) (C), radial damaged DNA (PDB ID: 1S75), (D) DNA:RNA hybrid (PDB ID: 479D), and (E) and (F) DNA adducts with drugs (PDB ID: 1HZ0 and 3LPV). Inter-probe distance PDFs were calculated using Eq. S3 based on accessible volumes derived using npsFRET tools (22). The difference between reference PDF corresponding to B-DNA and PDF corresponding to particular DNA model was quantified via Kolmogorov-Smirnov two-sample test (Tab S5). Length of DNA structures was, when necessary, adjusted using 3DNA program (48).

Table S5. Quantification of a distance between the "*in-cell*" PDFs simulated using npsFRET tools (22) for reference B-form of DNA and selected DNA models given in Figure S7 using Kolmogorov–Smirnov two-sample test. Identical distributions are marked by 0 value in the KS statistics. **T**he structural deformations represented by structures 1QUM, 479D, and 1LPV are expected to be distinguishable from canonical B-DNA even at the low precision of in-cell FRET. This assumption is based on ks2stat values equal or larger than the reference ks2stat value for B-A transition. Note that B-DNA could be successfully discriminated from A-DNA based on experimental *in-cell* spFRET data (Figure 3, Table 2).

PDB name	**A-DNA**	**Z-DNA**	**1QUM**	**1S75**	**479D**	**1HZ0**	**3LPV**
ks2stat	0.5900	0.3169	0.7838	0.1883	0.5990	0.3995	0.5857

Supplementary notes

To avoid the intrinsic cell fluorescence and to reduce the scattering of laser, which is dependent on wavelength of excitation source, in heterogeneous and highly dispersing cell environment, we used FRET pair shifted to far red and near infrared region (Fig. S8).

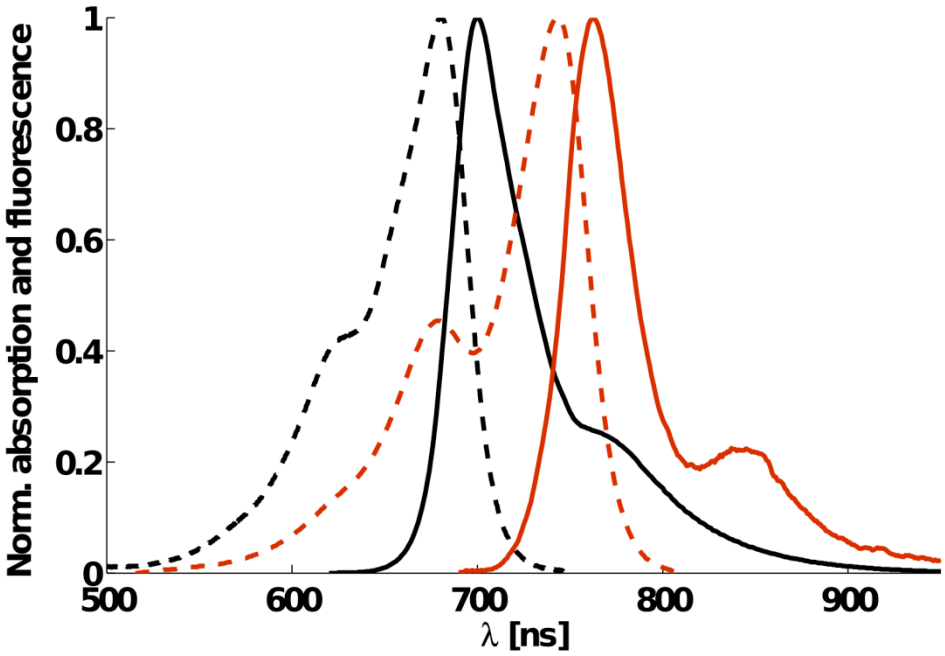

Figure S8. Absorption and fluorescence spectra of used FRET pair, ATTO680 absorption spectrum (black dashed line), ATTO680 fluorescence spectrum (black solid line), ATTO740 absorption spectrum (red dashed line) and ATTO fluorescence spectrum (red solid line).

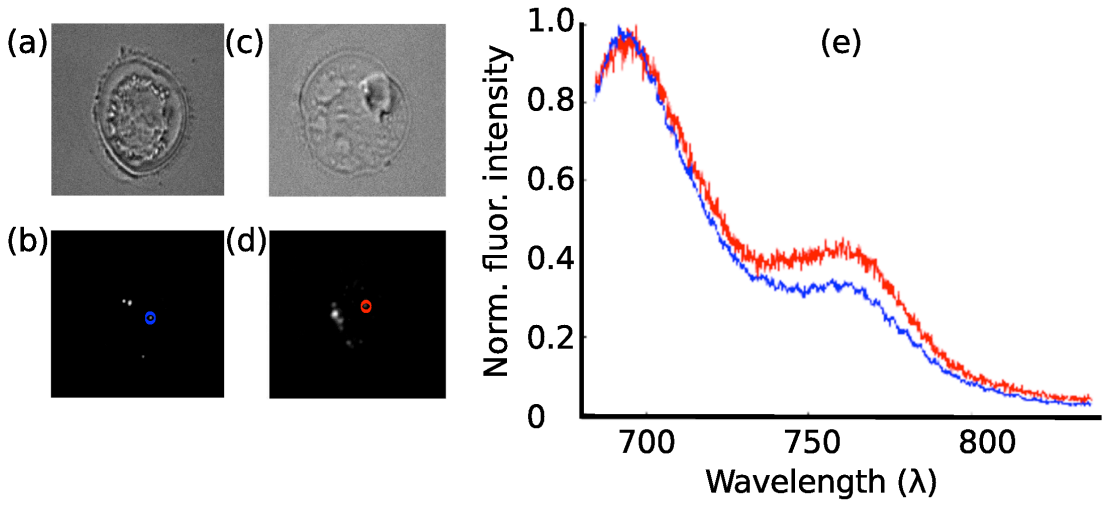

Figure S9. *In-cell* spFRET on labeled 14-mer DNA oligonucleotide inside human epitheloid carcinoma (HeLa) cells. (a) and (c) transmission images of HeLa cells after electroporation with the DNA constructs labeled with ATTO680 and the complete FRET pair (ATTO680 & ATTO740), respectively. (b) and (d) individual probed DNA molecules labeled with ATTO680 and the complete FRET pair, respectively. (e) The energy transfer between donor and acceptor of energy is revealed via normalized fluorescence spectra. Blue curve corresponds to molecule of DNA labeled with donor molecule in the absence of acceptor (incident molecule is highlighted by blue circle in subfigure *b*). Red curve corresponds to complete FRET pair (incident molecule is highlighted by red circle in subfigure *d*). Difference between normalized spectra in emission region of acceptor (ATTO740) indicates energy transfer between FRET probes terminally attached to 14-mer DNA oligonucleotide. Direct excitation of acceptor was usually undetectable in single-molecule fluorescent spectrum.

Intra-cellular localization and diffusion of DNA introduced into cells.

Inside the living cells, the behavior of introduced small oligo-nucleotides is not intuitive and differs from their behavior under in vitro conditions. It has been demonstrated that exogenous DNA molecules, as small as 20 nt, introduced into cytoplasm of living eukaryotic cells tend to spontaneously localize and concentrate in the nucleus within the few minutes (37-40). Inside the nucleus, even such small DNA fragments are virtually immobile (44). Of note, in nucleoplasm, the mobility of small DNA fragments was found to be virtually independent of DNA size (e.g. in nucleus of HeLa cells, the translational diffusion for ~20 nt long DNA fragment was found to be essentially identical to translational diffusion of 1000 nt long DNA fragment (44)). Although the mechanism of DNA immobilization remains unknown, there are several lines of experimental evidence indicating that the "immobilization" might be due to molecular crowding inside the nucleus and related local confinement as well as due to both specific and non-specific interactions with nuclear proteins (44).

It is expected that the free diffusing molecule should not be visible at the considered time-scale in a single molecule mode. In this respect, our observation of "*diffraction limited spot"* in HeLa cells agrees with above-mentioned notion of the DNA immobilization. Observation of "*diffraction limited spot"* in bacterial cell indicates that the DNA is immobilized

also in bacterial cells. The DNA immobilization in prokaryotic cell suggests that similar mechanisms, as those modulating translational diffusion in nucleus of eukaryotic cells, might function in nucleoid of bacterial cell.

Additional references:

44. Lukacs, G.L., Haggie, P., Seksek, O., Lechardeur, D., Freedman, N. and Verkman, A.S. (2000) Size-dependent DNA mobility in cytoplasm and nucleus. *J Biol Chem*, **275**, 1625-1629.

45. Sorokina, M., Koh, H.R., Patel, S.S. and Ha, T. (2009) Fluorescence lifetime trajectories of a single fluorophore reveal reaction intermediates during transcription initiation. *J Am Chem Soc*, **131**, 9630-9631.

46. Vishwasrao, H.D., Heikal, A.A., Kasischke, K.A. and Webb, W.W. (2005) Conformational dependence of intracellular NADH on metabolic state revealed by associated fluorescence anisotropy. *J Biol Chem*, **280**, 25119-25126.

47. Sullivan, M. (2011) Fundamentals of Statistics, 3rd Edition, Pearson Prentice Hall, USA, p. 118

48. Lu, X.-J. and Olson, W.K. (2003) 3DNA: a software package for the analysis, rebuilding and visualization of three-dimensional nucleic acid structures. *Nucl Acids Res*, **31**, 5108-5121.